Interannual covariability in Northern Hemisphere air temperatures and greenness associated with El Niño-Southern Oscillation and the Arctic Oscillation

Wolfgang Buermann,[1,2] Bruce Anderson,[1] Compton J. Tucker,[3] Robert E. Dickinson,[4] Wolfgang Lucht,[5] Christopher S. Potter,[6] and Ranga B. Myneni[1]

Received 7 June 2002; revised 5 November 2002; accepted 24 January 2003; published 15 July 2003.

[1] In this paper, we estimate the year-to-year variations in northern vegetation greenness as they relate to the dominant modes of climate variability. In particular, we analyze spatial data of Northern Hemisphere satellite-sensed vegetation greenness, surface temperature, precipitation, and upper air data for the 1982–1998 period to isolate well correlated modes of variability between temperature and greenness and to assess their relationship to large-scale circulation anomalies. It is found that during spring, large-scale modes of interannual vegetation variability are strongly correlated with spatiotemporal modes of variability in the overlying temperature field. In addition, the results indicate that the two predominant hemispheric-scale modes of covariability are related to teleconnections associated with the El Niño-Southern Oscillation (ENSO) and the Arctic Oscillation (AO). The warm event ENSO signal is manifested as warmer and greener conditions in North America, Far East Asia, and to some extent central Europe, while the features of the positive phase AO signal include enhanced warm and green conditions over large regions in Europe and Asian Russia, with opposite anomalies in the eastern half of North America. Whether observed trends in vegetation activity over the past 20 years are also related to systematic changes in these two modes of variability is still unclear. *INDEX TERMS:* 1620 Global Change: Climate dynamics (3309); 1640 Global Change: Remote sensing; 3322 Meteorology and Atmospheric Dynamics: Land/atmosphere interactions; *KEYWORDS:* NDVI, Temperature, ENSO, AO, interannual variability, canonical correlation analysis

Citation: Buermann, W., B. Anderson, C. J. Tucker, R. E. Dickinson, W. Lucht, C. S. Potter, and R. B. Myneni, Interannual covariability in Northern Hemisphere air temperatures and greenness associated with El Niño-Southern Oscillation and the Arctic Oscillation, *J. Geophys. Res.*, *108*(D13), 4396, doi:10.1029/2002JD002630, 2003.

1. Introduction

[2] Vegetation covers nearly three-fourths of the Earth's land surface and plays a key role in global energy, hydrological and biogeochemical cycles. Therefore it is important to know and understand changes in vegetation activity, particularly with relation to changes in near-surface climate variables such as air temperature [*Zhou et al.*, 2001]. The importance of spring and early summer temperatures in initiating and determining growing season photosynthetic gain of vegetation at midlatitudes and high latitudes is well known [*Goulden et al.*, 1998; *Vaganov et al.*, 1999; *Barford et al.*, 2001]. One may expect some modulation of this temperature sensitivity, depending on the vegetation type, nutrient availability, precipitation, etc. [*Braswell et al.*, 1997; *Jarvis and Linder*, 2000; *Barber et al.*, 2000].

[3] Interestingly, near-surface air temperature records of the past 25 years suggest a rate of warming greater than in any previous period of the instrumental record [*Folland et al.*, 2001], and possibly the last millennium [*Mann et al.*, 1999]. The warming was pronounced in the northern latitudes, especially during the winter and spring seasons [*Hansen et al.*, 1999]. Consistent with this warming in the north are several reports of increased vegetation greenness [*Keeling et al.*, 1996; *Myneni et al.*, 1997; *Tucker et al.*, 2001] and changing phenology [*Colombo*, 1998; *Schwartz*, 1998; *Bradley et al.*, 1999; *Menzel and Fabian*, 1999; *Chmieliewski and Roetzer*, 2002], and poleward range extensions by birds [*Thomas and Lennon*, 1999] and butterflies [*Parmesan et al.*, 1999]. The northern latitude greening reports are thus especially intriguing because such changes can potentially feedback on climate [*Buermann et al.*, 2001] and can also provide insight in to the carbon budget closure issues [*Myneni et al.*, 2001].

[1]Department of Geography, Boston University, Boston, Massachusetts, USA.
[2]Now at Center for Atmospheric Sciences, University of California, Berkeley, Berkeley, California, USA.
[3]Biospheric Sciences Branch, NASA Goddard Space Flight Center, Greenbelt, Maryland, USA.
[4]School of Earth and Atmospheric Sciences, Georgia Institute of Technology, Atlanta, Georgia, USA.
[5]Potsdam Institute for Climate Impact Research, Potsdam, Germany.
[6]Ecosystem Science and Technology Branch, NASA Ames Research Center, Moffett Field, California, USA.

0148-0227/03/2002JD002630$09.00

[4] In an attempt to investigate this issue, *Zhou et al.* [2001] documented a statistically significant relation between changes in surface temperature and satellite-measured vegetation greenness for the spring and growing seasons during the 1980s and 1990s. This relationship, however, was established only for large area averages (40°N to 70°N) over North America and Eurasia. It is well known that climate parameters such as surface temperature do not show spatially homogeneous variations over time but instead display coherent patterns of spatial heterogeneity related to hemispheric-scale circulation features, for example the El Niño-Southern Oscillation (ENSO) and the Arctic Oscillation (AO) [*Trenberth and Paolino*, 1981; *Thompson and Wallace*, 1998]. In fact, the unprecedented surface warming of the past 25 years was neither spatially nor seasonally uniform [*Hansen et al.*, 1999; *Folland et al.*, 2001], in part because of modulation by the ENSO and AO. In particular, warm ENSO events were relatively more frequent, persistent, or intense compared to a record dating back as far as 1882 [*Trenberth and Hoar*, 1997] while the AO positive phase occurred more frequently, resulting in an overall increase in the average AO index [*Thompson et al.*, 2000].

[5] In this context, the *Zhou et al.* [2001] analysis raises two questions: (i) Is the correlation between northern vegetation greenness and temperature valid at all spatial and temporal scales? and, (ii) Can we estimate the component of the year-to-year variations in northern vegetation greenness that is due to temperature variations associated with the dominant modes of climate variability?

[6] To answer these questions we performed a canonical correlation analysis [*Barnett and Preisendorfer*, 1987] on spring land surface temperature and vegetation greenness data for the period 1982 to 1998. Canonical correlation analysis (CCA) is found to be most appropriate when the behavior of the statistical fields are governed by only a few multifaceted patterns such as is the case with ENSO or AO. The paper is organized as follows: the data and methods used are described in section 2, and the results are described in section 3. We conclude with a discussion in section 4 and a brief summary of the results in section 5.

2. Data and Methods

2.1. Data

[7] The greenness data are normalized difference vegetation index (NDVI) data processed by the Global Inventory Monitoring and Modeling Systems (GIMMS) group from measurements taken by the Advanced Very High Resolution Radiometers on NOAA satellites [*Tucker et al.*, 2003]. The NDVI captures the contrast between red and near-infrared reflectance of vegetation, which is indicative of the abundance of green leaf area [*Myneni et al.*, 1995]. Residual non-vegetation effects were noted in the data due to lack of an explicit atmospheric correction for tropospheric aerosols, water vapor absorption, surface anisotropy, etc. [*Zhou et al.*, 2001; L. Zhou et al., Relation between interannual variations in satellite measures of vegetation greenness and climate between 1982 and 1999, submitted to *Global Biogeochemical Cycles*, 2002] (hereinafter referred to as Zhou et al., submitted manuscript, 2002). To minimize such effects, *Los et al.* [2000] developed a four-step procedure, which involved a Fourier adjustment of outliers in the time series, Solar zenith angle correction, Interpolation for missing data, and Reconstruction of NDVI values over tropical rain forests (FASIR). These corrections were applied to the GIMMS NDVI data to produce a 1x1 degree global, monthly data set for a 17 year period, January 1982 to December 1998. This fourth generation data set overcomes most problems noted in previous generations of NDVI data sets [*Kaufmann et al.*, 2000; *Los et al.*, 2000; *Zhou et al.*, 2001; Zhou et al., submitted manuscript, 2002] and was therefore used in our study.

[8] The temperature data used in this study are 2×2 degree gridded monthly near-surface air temperature anomalies over land [*Hansen et al.*, 1999]. The data set is derived from measurements taken at rural and small towns. In addition, we employed monthly 250 mbar geopotential height data at 2.5×2.5 degree resolution (equivalent to a grid point spacing of approximately 250 km) from the reanalysis product developed by the National Centers for Environmental Prediction. Details about this data set, including its physics, dynamics and computational methods are discussed by *Kalnay et al.* [1996]. For supplementary analyses, we also utilized the 2.5×2.5 degree gridded monthly precipitation data set from the Climate Prediction Center Merged Analysis of Precipitation [*Xie and Arkin*, 1997]. Over land these fields are mainly derived from gauge observations.

2.2. Methods

2.2.1. Simple Correlation Analysis

[9] As a first step, we computed the grid point correlations between seasonal averages of Northern Hemisphere (NH) temperature as well as NDVI anomalies and indices that represent ENSO and AO variability for the 17 year study period 1982 to 1998. This analysis has the advantage of directness and simplicity in bringing forth any potential spatial patterns of direct and lagged correlation between these circulation anomalies and NH temperature or NDVI. Obviously, one cannot establish any linkage between the temperature and NDVI fields at this stage, but the results will guide further analysis. The seasons were defined as follows: winter as December to February, spring as March to May, summer as June to August and autumn as September to November. Seasonal averages were evaluated for pixels with at least two months of valid data. The data were detrended prior to simple correlation analysis to reduce the likelihood of spurious correlations.

[10] For ENSO, we correlated seasonal NH land surface temperature and NDVI anomalies at zero and various lags with the autumn NINO3 index. NINO3 is the sea surface temperature (SST) anomaly from the 5°S to 5°N and 90°W to 150°W region in the equatorial tropical Pacific [*Reynolds and Smith*, 1994]. The September to November NINO3 index is a good proxy for ENSO, as the SST anomalies then approach peak values during an ENSO cycle [e.g., *Dai et al.*, 1997]. With regard to the AO, *Thompson and Wallace* [1998] have documented the dominant impact of AO related variability on NH winter and springtime surface air temperatures. More recently, the same authors provided evidence that this mode is also present year-round but markedly weaker during the NH warm seasons [*Thompson and Wallace*, 2000]. In contrast to ENSO, the AO, which has a characteristic timescale of 10 days, does not necessarily have a long memory in the atmosphere [*Thompson and*

Wallace, 2002]. However, in our analysis, we also found that hemispheric-scale temperatures and NDVI fields are not necessarily best correlated with the contemporaneous seasonal AO index but instead, for certain seasons, they may actually be better correlated with preceding values of the AO index (not shown). Therefore, in order to identify the highest-correlated AO-related signal within the seasonal NH temperature and NDVI fields we performed correlations between these fields and three-month averages of the AO index (defined as the leading mode of NH sea level pressure fields [*Thompson and Wallace*, 1998]), starting one season prior to the temperature/NDVI fields and proceeding through the three-month period concurrent with the seasonal-mean fields. We then selected the three-month average AO value that showed the highest hemispheric correlation with the seasonal field under consideration (either temperature or NDVI), not necessarily the concurrent AO value, and used its time series to define the time-evolution of the AO-related influence for that season. Importantly, in the case of the NH winter, spring and summer seasons both temperature and NDVI fields correlate most strongly with the same three-month periods, allowing us to use the same AO index period for each. Only in the NH fall season does it appear that the NDVI and temperature fields are related to slightly differing periods of the AO (fall temperatures correlate most strongly with the preceding summer AO, whereas fall NDVI correlates more strongly with fall AO). Although of interest, investigation into the reason for the apparent lag between the AO pattern and the hemispheric-scale temperature (and NDVI) signal is beyond the scope of this paper, which is instead more concerned with identifying modes of hemispheric-scale covariability in the temperature and NDVI fields themselves.

[11] Throughout the paper, correlation maps are used to identify regions of variability within the temperature and NDVI fields. In order to estimate significance for these correlation values, we assumed that each season represents an independent event within a normalized distribution. For the 17-year study period under consideration, this results in 15 degrees of freedom with corresponding significance levels of 0.41 (90%) and 0.48 (95%) (based on a two-tailed *t* statistics). It should be noted that we have also repeated this analysis using precipitation fields (see Appendix B).

2.2.2. Canonical Correlation Analysis

[12] In order to more explicitly highlight the linkage between near-surface climate and vegetation activity, we also used a multivariate data-reduction technique in order to identify and isolate well correlated modes of spatiotemporal variability between temperature and NDVI on regional to hemispheric scales. Once these modes have been independently identified, they can then be used to analyze the relationship between the coupled patterns and larger-scale circulation anomalies. With this objective in mind, we performed a canonical correlation analysis in which the predictor fields are NH (10°N to 90°N) land surface temperature anomalies and the predictand fields are NH (10°N to 90°N) NDVI anomalies [*Barnett and Preisendorfer*, 1987]. We shall focus on the springtime within the 17 year study period (1982 to 1998) because of the sensitivity of plant growth to temperature.

[13] The CCA performed here is designed to select those temporal features in the greenness fields that are best correlated with temporal features in surface temperature fields. The algorithm used is similar in nature to a simple empirical orthogonal function (EOF) analysis, although the field on which the single value decomposition is performed differs in that it contains a cross-correlation matrix relating a predictand field to a predictor field. In particular, the algorithm attempts to minimize the variance between a subset of the NDVI and temperature EOF time series to produce a set of canonical factor (CF) time series that isolate modes of greatest correlation within the two data sets (as opposed to isolating modes of greatest variance explained as in the case of EOF [*Barnett and Preisendorfer*, 1987]). The subset of EOFs used for CCA was limited to the first six for temperature and NDVI. Together, they explain 76% (64%) of NH spring temperature (NDVI) variability (for more details see Appendix A).

[14] The CCA produces two weighting matrices, one for the temperature EOFs and one for the NDVI EOFs, that are used to reconstruct the temporal factors from the original EOF time series. It also produces an eigenvalue matrix representing the squared correlation between the temporal factors. These eigenvalues (Table 1) suggest that the first three factor correlations are very high ($r > 0.9$). The next two factor correlations are reasonable, but the last is weaker. The robustness of the CFs was assessed by systematically varying the number of EOFs retained prior to CCA. This exercise indicated that the first two CFs are robust. The higher-order CFs exhibited some sensitivity to the effects of EOF truncation and also, in some instances, appeared to isolate single, unique events, such as the extraordinary warmth of 1997 (third CF) and the impact of the Mount Pinatubo eruption in 1991 (fifth CF) on land temperatures and vegetation greenness (not shown).

[15] Isolating single, extreme events in conventional CCA is generally avoided by reducing the number of EOFs retained [*Feddersen et al.*, 1999]. This was not possible in our case for two reasons: (a) the relatively short record length of only 17 years and (b) such events appear to explain a significant portion of the variance (Table 1). Hence, in the following section, we present results of a detailed analysis only for the first two CFs.

[16] To further diagnose the results, we correlated the time series of the first two temperature CFs with the contemporaneous spring 250 mbar geopotential height fields over the study period 1982 to 1998. The upper air geopotential height fields characterize large-scale and free atmospheric dynamics associated with major steering patterns; in addition, interannual climate variability can be seen in the displacement and strengthening of this field.

3. Results

3.1. Simple Correlation

3.1.1. El Niño-Southern Oscillation

[17] The ENSO phenomenon is commonly understood as anomalously warm or cool surface waters in the eastern tropical Pacific ocean but actually involves many other changes in both the atmosphere and the ocean far away from the center of action [e.g., *Trenberth and Paolino*, 1981]. The changes in SSTs and associated deep convection perturb the local Hadley circulation and produce anomalous upper tropospheric divergence in the tropics and convergence in the subtropics [*Trenberth et al.*,

Table 1. Eigenvalues and Variances Explained by Canonical Correlation Analysis of Spring NH (10°N to 90°N) Land Surface Temperature and NDVI Anomalies[a]

		Explained Variance, %	
Factor	Eigenvalue	Temperature	NDVI
1	0.96	10.8	13.5
2	0.91	18.4	9.9
3	0.87	11.0	14.9
4	0.61	13.1	9.1
5	0.56	13.0	8.7
6	0.3	9.6	8.0

[a]The eigenvalues represent the squared correlation between the reconstructed temporal canonical factors of temperature and NDVI.

1998]. These changes in the upper atmosphere provide the sources for large-scale atmospheric Rossby waves through which the ENSO signal is thought to propagate toward higher latitudes [*Hoskins and Jin*, 1991]. The resulting alterations in the extra-tropical atmospheric circulation causes changes in storm tracks, temperature and precipitation fields [*Trenberth et al.*, 1998]. These ENSO related extra-tropical teleconnection patterns, as captured by the Pacific North American (PNA) pattern [*Wallace and Gutzler*, 1981], are typically strongest in the winter and most pronounced over North America [*Horel and Wallace*, 1981].

[18] To illustrate the seasonal impact of the ENSO signal, we correlated seasonal land surface temperature and NDVI anomalies with the autumn NINO3 index (Figures 1 and 2). The influence of ENSO teleconnections on surface temperatures in North America is apparent from Figure 1. The northwest regions during the warm ENSO events experience moderate warming in the fall, which intensifies in the winter, when it covers much of the continent. The warming moderates by spring and is confined to the north. Cooler conditions are observed in the southwest. Eurasian temperature fields are only weakly correlated with the ENSO index. Some warming may be noted in Europe during the warm events in the fall and winter. In summer, several regions of the NH continents show slightly warmer conditions. These patterns generally resemble composites of temperature changes assembled from longer time series [*Halpert and Ropelewski*, 1992], suggesting that the 17 year period of our study, although short, may nevertheless be representative. The corresponding correlations with NDVI, shown in Figure 2, suggest enhanced greenness in all seasons over large parts of North America during the warm events. This can be attributed principally to warmer cold seasons in the boreal and temperate regions. Enhanced spring greenness in the southwest is likely because of enhanced cold season precipitation in these water limited regions (Appendix B; also *Trenberth and Caron* [2000]). The weak ENSO and NDVI relations in Eurasia are consistent with ENSO and temperature patterns (Figure 1). There are indications of temperature- and precipitation-linked greenness changes over parts of Europe as well as in central and Far East Asia in spring and summer (see also Appendix B).

3.1.2. Arctic Oscillation

[19] The AO has a dominant influence on the NH near-surface climate [*Thompson and Wallace*, 1998]. This predominantly zonally symmetric hemispheric mode of variability, most active in winter, is characterized by a seesaw of atmospheric mass between the polar cap and the middle latitudes in both the Atlantic and Pacific Ocean basins. The AO positive phase relates to lower-than-normal pressure over the polar region and higher-than-normal pressure at about 45 degrees north latitude, thereby steering ocean storms farther north and favoring zonal advection of relatively warm and wet air deep into continental interiors [*Thompson and Wallace*, 2000]. The negative phase brings the opposite conditions. The better known North Atlantic Oscillation is now viewed as a regional manifestation of the same physical phenomena that underlies the larger-scale AO [*Hurrell*, 1995; *Wallace*, 2000]. *Thompson and Wallace* [1998] suggest that intraseasonal, interannual and interdecadal variability in the AO is linked to strong fluctuations in the NH lower stratospheric polar vortex. The ensuing cooling of the lower stratosphere and strengthening of the polar vortex over the last 30 years is speculated to have driven the AO more frequently into its positive phase [*Thompson and Wallace*, 1998].

[20] The spatial patterns of simple correlation between seasonal temperature anomalies and seasonal averages of the AO index demonstrate the dominant influence of the AO on NH surface temperatures, especially in the winter and spring periods (Figure 3). The winter pattern, which is most strongly correlated with the concurrent DJF AO index, shows a broad belt of warming in northern Eurasia and a moderate warming over southeastern North America, and cooling in Africa, the Indian subcontinent and northeastern North America during the positive phase. The spring pattern, which is most strongly correlated with the preceding JFM AO index, closely resembles the winter pattern except that the cooling center of action over the eastern half of North America has expanded southward. Aside from the cooler conditions during spring over eastern North America, these cold season patterns are generally consistent with those derived from a longer data series [*Thompson and Wallace*, 1998, 2000]. The influence of the AO upon surface temperatures is weaker in the NH warm seasons. In fall, however, a pattern of moderate warming over Eurasian high latitudes and slight cooling over Eurasian low latitudes and Africa during the positive phase of the preceding JJA Arctic Oscillation is evident. The correlation patterns between the AO index and NDVI anomalies, shown in Figure 4, are consistent with the patterns between the AO index and surface temperature (Figure 3). These patterns are spatially more coherent in the spring period, when warmer temperatures in Eurasia are linked to enhanced greenness, while cooler temperatures in the eastern half of North America are related to decreased greenness (in the positive phase). In contrast, the decline in greenness in central Europe during the summer is possibly more a result of reduced summer time precipitation associated with the positive phase of the AO (Appendix B).

3.2. Canonical Correlation

3.2.1. First Canonical Factor: ENSO Mode

[21] The temporal and spatial patterns of the first canonical factor, as derived from the canonical correlation analysis described above, are shown in Figure 5. This figure indicates that the first factor captures the NH spring ENSO teleconnection signal in the surface temperature and NDVI

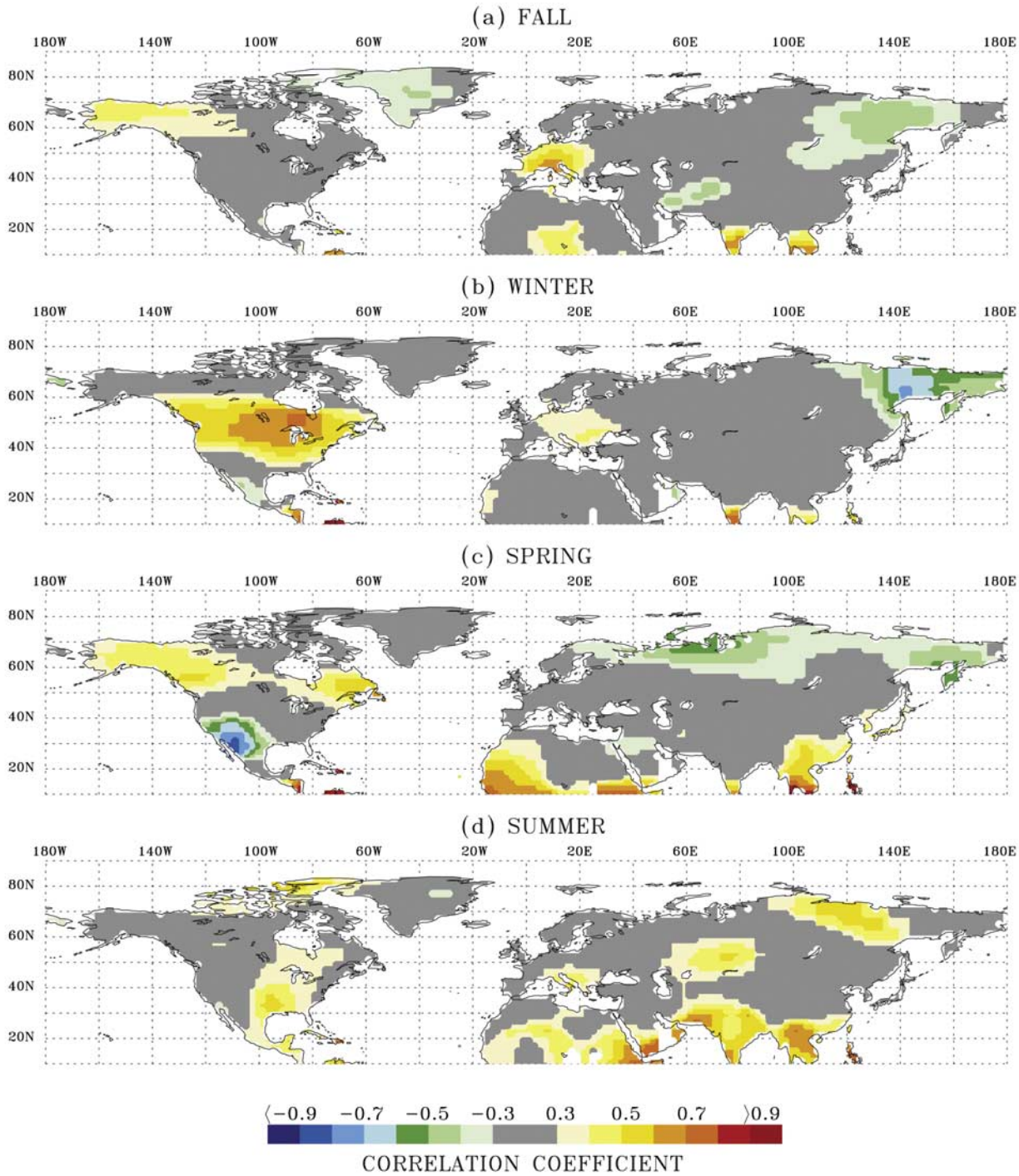

Figure 1. Patterns of simple correlation between September through November (SON) average NINO3 index and land surface temperature anomalies for the period 1981/1982 to 1997/1998. The four panels depict the correlation pattern between the 1981 to 1997 SON NINO3 and (a) 1981 to 1997 September through November average temperature anomalies, (b) 1982 to 1998 December through February average temperature anomalies, (c) 1982 to 1998 March through May average temperature anomalies, and (d) 1982 to 1998 June through August average temperature anomalies. Land areas not contoured indicate missing data. Because of the 17 year study period, the significance level for correlations is 0.41 (90%) and 0.48 (95%).

fields. In particular, the spatial patterns closely resemble patterns of simple correlation between the ENSO index and spring temperature (Figure 1c) and spring NDVI (Figure 2c). In addition, the time series of temperature and NDVI CFs are significantly correlated with the time series of the NINO3 index (Figure 5a). These ENSO related patterns explain 10.8% (13.5%) of the total spring surface temperature (NDVI) variability (Table 1).

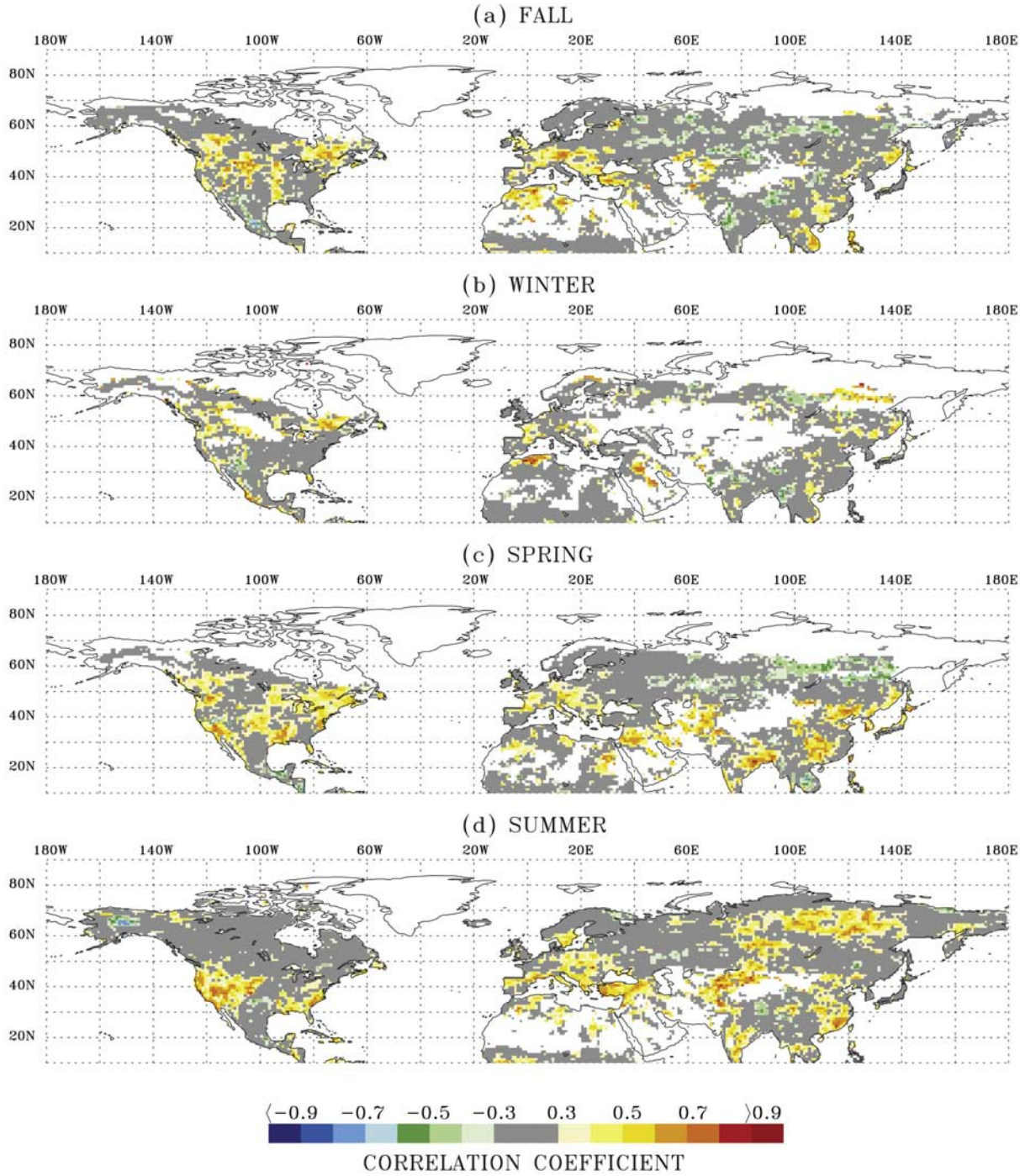

Figure 2. Patterns of simple correlation between September through November average NINO3 index and NDVI anomalies for the period 1981/1982 to 1997/1998. (a) 1982 to 1997 September through November average NINO3 and 1982 to 1997 September through November average NDVI anomalies, 1981 to 1997 September through November average NINO3 and (b) 1982 to 1998 December through February average NDVI anomalies, (c) 1982 to 1998 March through May average NDVI anomalies, and (d) 1982 to 1998 June through August average NDVI anomalies. Land areas not contoured indicate missing data.

[22] The spatial patterns associated with this mode, shown in Figures 5b and 5c, reveal certain interesting details. The warmer and greener regions in North America and Far East Asia are more strongly coupled and spatially coherent than in patterns of simple correlation (Figures 1c and 2c). The temperature-greenness linkage in precipitation limited regions of the southwest of North America and in central Asia seen previously is now de-emphasized. The

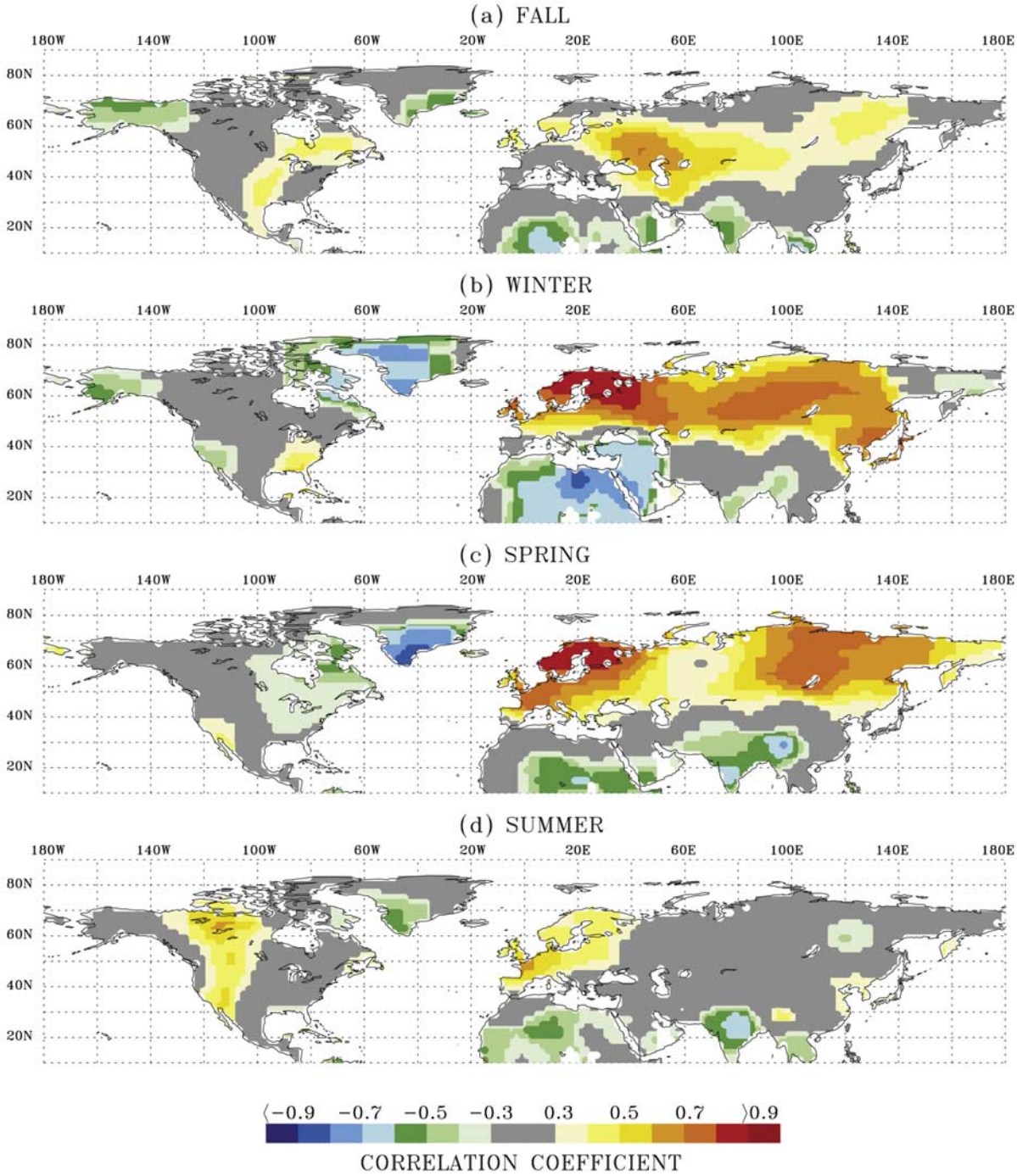

Figure 3. Patterns of simple correlation between three-month averages of the Arctic Oscillation (AO) index and land surface temperature anomalies for the period 1981/1982 to 1997/1998 (see text for details). (a) September through November average temperature anomalies correlated with the JJA AO index for 1981 to 1997, (b) December through February average temperature anomalies correlated with the DJF AO index for 1982 to 1998, (c) March through May average temperature anomalies correlated with the JFM AO index for 1982 to 1998, and (d) June through August average temperature anomalies correlated with the JJA AO index for 1982 to 1998. Land areas not contoured indicate missing data.

temperature sensitivity is biome-specific, as it is manifested more strongly and coherently in areas dominated by grasslands and broad leaf forests in North America and Far East Asia. Finally, many spatial features seen in the winter patterns of simple correlation (Figures 1b and 2b) are also seen in the spring canonical patterns (Figures 5b and 5c), suggesting that contemporaneous vegetation greenness may also be an integrated expression of recent past temperature

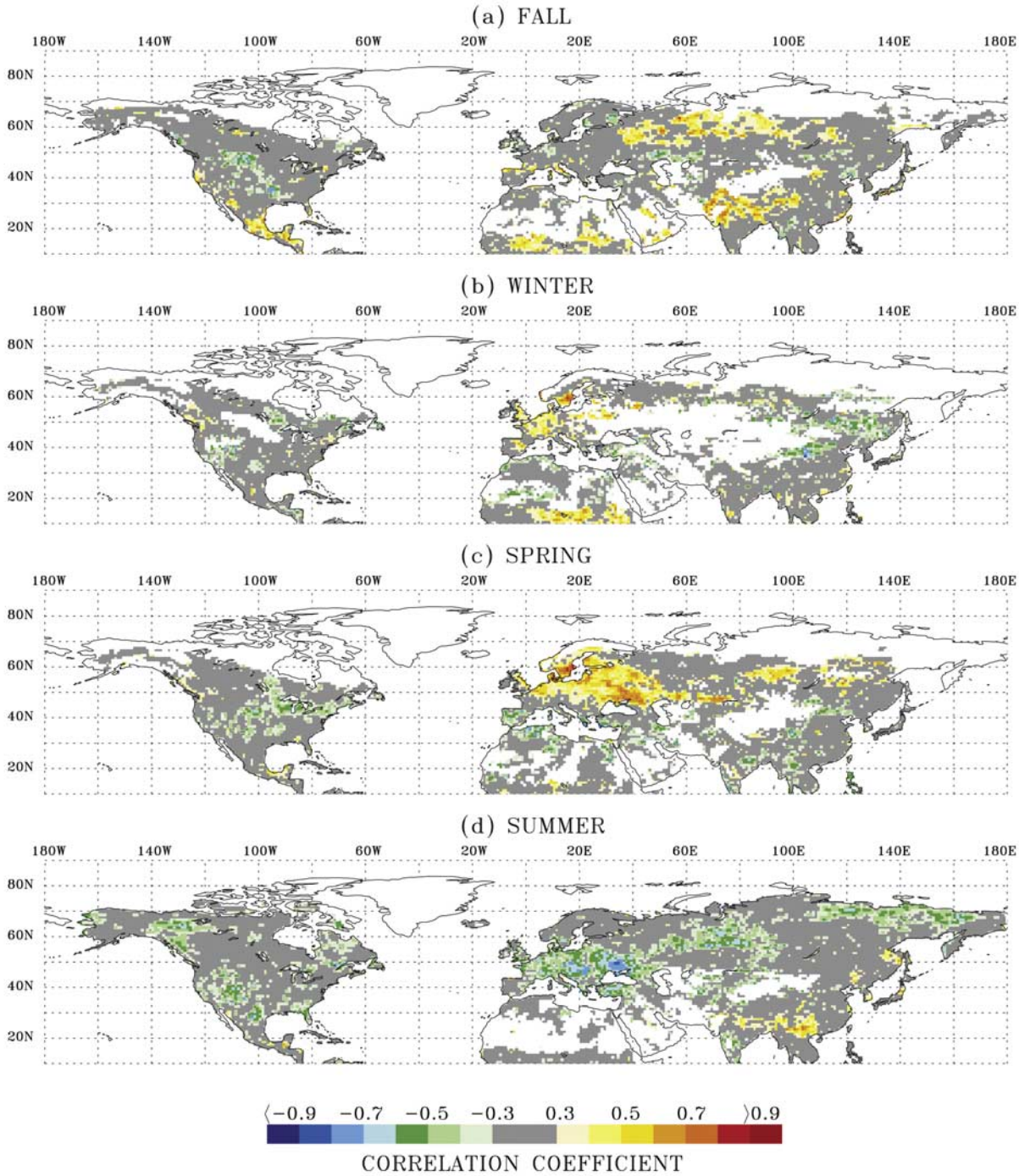

Figure 4. Patterns of simple correlation between three-month averages of the Arctic Oscillation (AO) index and NDVI anomalies for the period 1982 to 1997/1998. (a) September through November average NDVI anomalies correlated with the JJA AO index for 1982 to 1997, (b) December through February average NDVI anomalies correlated with the DJF AO index for 1982 to 1998, (c) March through May average NDVI anomalies correlated with the JFM AO index for 1982 to 1998, and (d) June through August average NDVI anomalies correlated with the JJA AO index for 1982 to 1998. Land areas not contoured indicate missing data.

conditions. In particular, the enhanced spring greenness in Europe during warm events seems more attributable to milder preceding winter temperatures and possibly increased spring precipitation (see Appendix B).

[23] It is important to note that CCA is designed to isolate the best-correlated modes of temperature/greenness covariability, not necessarily the modes that explain the largest amount of variance (or covariance). As such, it is possible

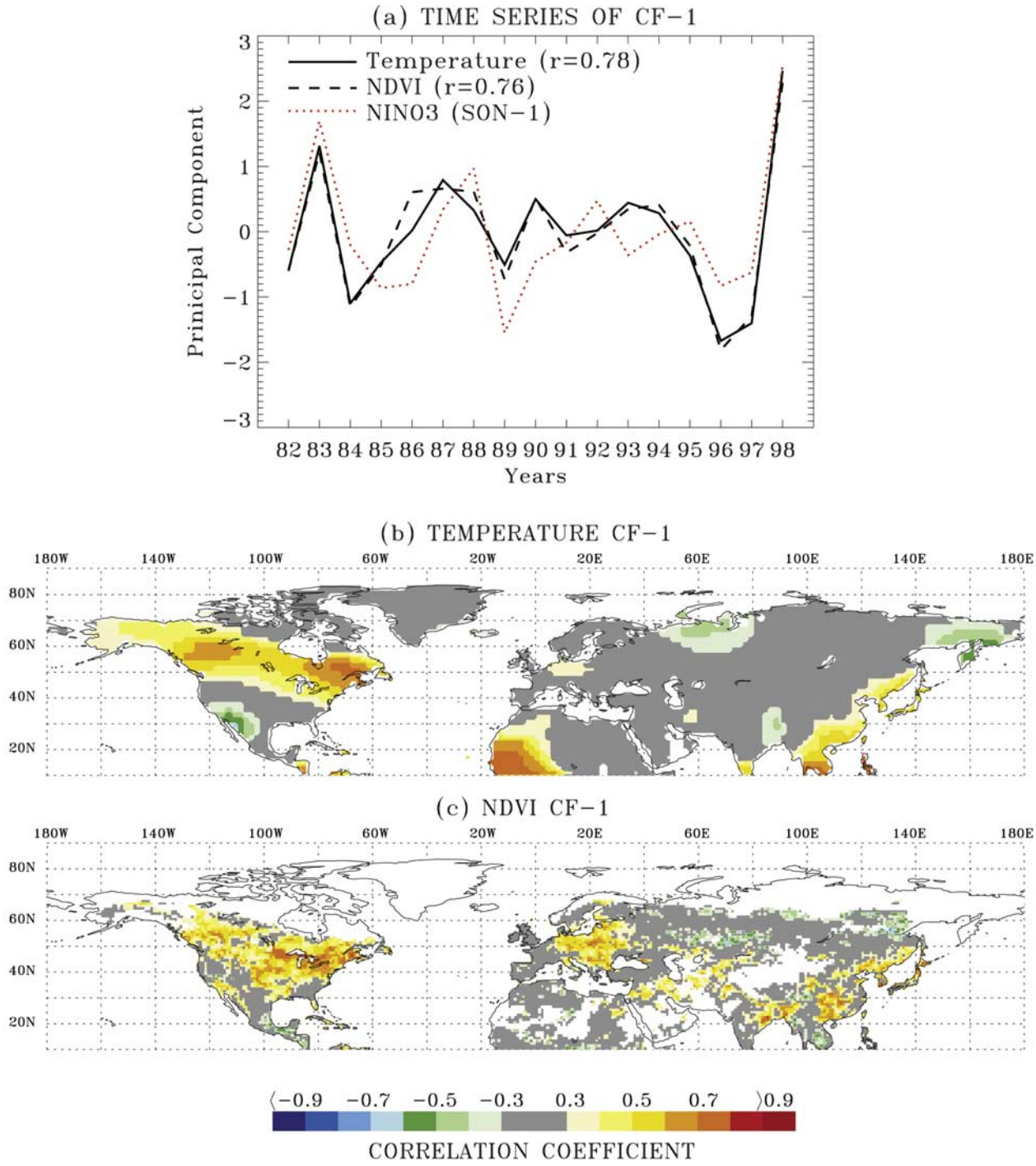

Figure 5. (a) Normalized time series of the first canonical factor of spring Northern Hemisphere (10°N to 90°N) land surface temperature and NDVI anomalies for the 17 year period of record, 1982 to 1998. The standardized September through November average NINO3 index time series of the preceding year is also shown in this plot (red dotted line). (b and c) Corresponding spatial patterns of correlation between the time series of the respective canonical factors and the data, shown in Figures 5b for temperature and 5c for NDVI.

for the CCA algorithm to isolate patterns within the temperature/greenness fields that may have well correlated features but that do not explain much variance in the overall system. The fact that there is quantitative agreement between the temporal and spatial features isolated via the CCA algorithm and those associated with ENSO (and AO, in the next section) indices suggests that surface temperature signatures associated with these two predominant modes of

global climate variability are also important drivers for variability in Northern Hemisphere greenness.

[24] Next we investigated how the upper-air patterns associated with these known modes of hemispheric-scale climate variability are related to the low-level temperature and greenness fields isolated through the CCA. The grid point covariance values between the time series of the first CF of temperature and the time series of NH spring 250 mbar geopotential height anomalies [*Kalnay et al.*, 1996] are shown in Figure 6. This upper air correlation pattern suggests the existence of a planetary wave train originating from over the eastern equatorial Pacific similar to that associated with ENSO-like tropical large-scale boundary forcing [*Horel and Wallace*, 1981]. In addition, there appears to be a secondary influence related to variability in the region of the East Asian jet. ENSO-related variability in the East Asian jet has previously been documented [*Wang et al.*, 2000]. This variability appears to be related to changes in the upper-level divergent circulation that link anomalies over the East Asian monsoon with ENSO-related changes in convective activity over the western and central equatorial Pacific. Importantly, this variability in the East Asian jet has also been related to warmer springtime conditions, in agreement with results shown here [*Wang et al.*, 2000].

[25] Previous researchers have shown that additional linkages between the upper-air teleconnection features and surface temperature signatures are associated with changes in storm tracks, surface fluxes, baroclinic wave activity, and blocking patterns [*Trenberth and Hurrell*, 1994; *Kiladis and Diaz*, 1989; *Bonsal et al.*, 2001; *Fraedrich*, 1994]. In addition, warmer conditions at the surface (Figure 5b) are co-located with positive height anomalies (Figure 6), and vice versa, which is consistent with the equivalent barotropic nature of climate anomalies in the midlatitude regions [*Gill*, 1982]. Hence it appears that the upper-air teleconnection patterns provide a bridge between the remote forcing fields and the surface temperature and NDVI fields. In the case of ENSO forcing, the relative warming of the sea surface over the eastern equatorial Pacific alters the upper atmospheric circulation in the equatorial Pacific [*Arkin*, 1982]. These anomalies then propagate into the sub-tropical and extra-tropical latitudes via Rossby wave dynamics, producing large-scale changes in upper air patterns over the Pacific, North America, the Atlantic and Europe [*Hoskins and Jin*, 1991]. Through dynamic mechanisms mentioned above, these upper air patterns can then influence variations in the surface temperature fields and contemporaneous variations in Northern Hemisphere greenness.

3.2.2. Second Canonical Factor: AO Mode

[26] The temporal and spatial patterns of the second canonical factor, shown in Figure 7, suggest that this factor represents a NH spring AO teleconnection signal in surface temperature and NDVI fields. In particular the spatial patterns closely resemble patterns of simple correlation between the winter (JFM) AO index and spring temperature/NDVI (Figures 3c and 4c); in addition, the time series of the temperature/NDVI CFs are significantly correlated with the time series of the winter (JFM) AO index (Figure 7a). These AO related patterns explain 18.4% (9.9%) of the total spring surface temperature (NDVI) variability (Table 1).

[27] The main spatial features associated with the positive phase of the AO during NH spring appear to be enhanced

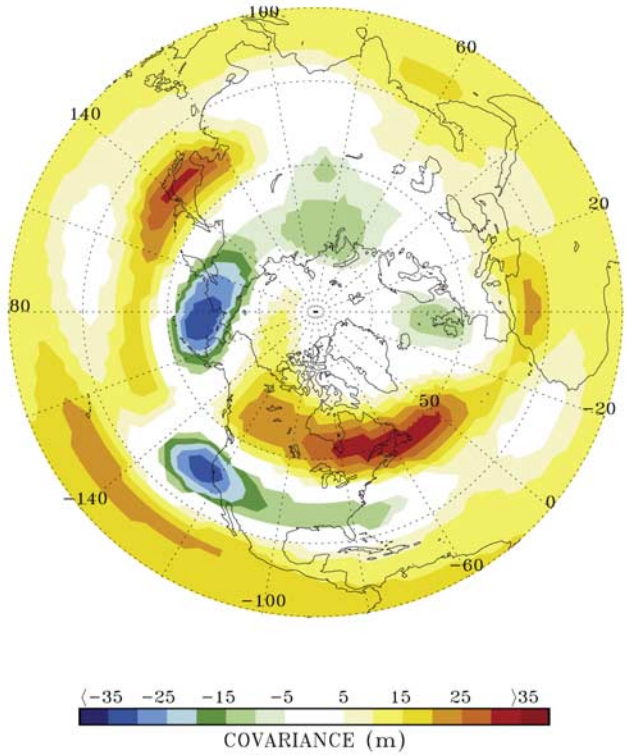

Figure 6. Correlations between spring 250 mbar geopotential height anomalies and the first temporal canonical factor of spring land surface temperature anomalies for 1982 to 1998.

warm and green conditions over large regions in Europe and Asian Russia with the opposite conditions in the eastern half of North America. The canonical patterns especially highlight regions where vegetation sensitivity to temperature is strong. For example, the center of action of the temperature signal in Europe (associated with the positive phase) is expanded south and westward compared to the AO correlation pattern (Figure 3c). Biome dependency in vegetation response to temperature variations associated with the AO may also be inferred from the spatial patterns shown in Figure 7. The temperature sensitivity is manifested more cleanly in the grasslands and broad leaf forests of eastern Europe and in parts of North America.

[28] The respective correlations of the 250 mbar geopotential height anomalies with the time series for the second CF of surface temperatures are shown in Figure 8. The similarity of this pattern with recently published AO related upper air regression maps provides further evidence that the second CF represents an AO teleconnection signal with its origin in the polar regions [*Thompson and Wallace*, 1998]. As seen before, warmer (cooler) surface conditions are associated with positive (negative) height anomalies, again indicating that there is an equivalent barotropic structure to the overlying atmosphere [*Thompson and Wallace*, 2000]. Although the theories for formation and evolution of the AO are not as well developed as those for ENSO, it appears that as with ENSO, the upper atmospheric patterns serve as a bridge for the teleconnection pattern, allowing it to influence hemispheric-scale regions. This influence is then transmitted to the surface temperature

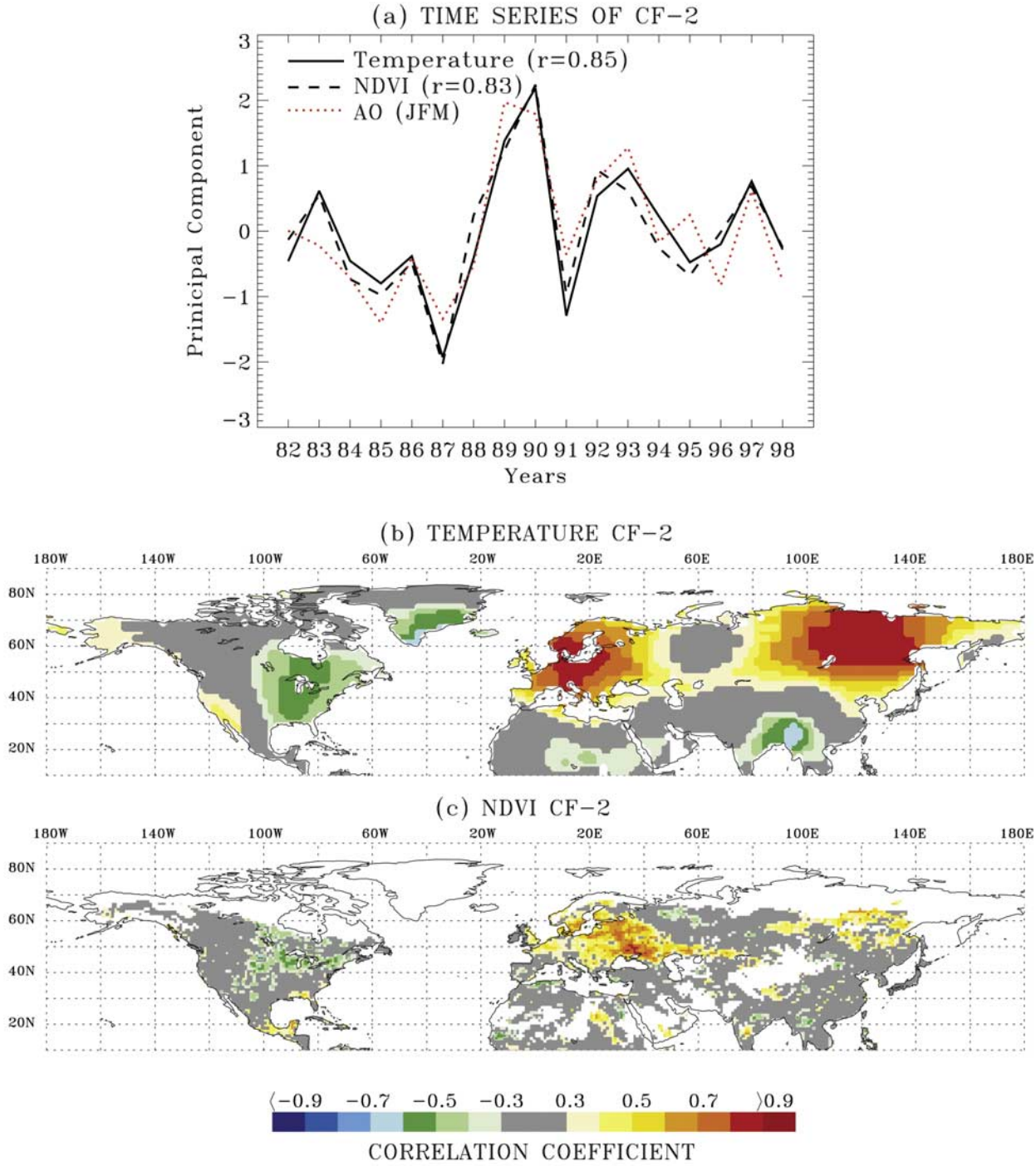

Figure 7. (a) Normalized time series of the second canonical factor of spring Northern Hemisphere (10°N to 90°N) land surface temperature and NDVI anomalies for the 17 year period of record, 1982 to 1998. The standardized January through March average Arctic Oscillation index time series is also shown in this plot (red dotted line). (b and c) Corresponding spatial patterns of correlation between the time series of the respective canonical factors and the data, shown in Figures 7b for temperature and 7c for NDVI.

and NDVI fields via the dynamic response of the atmosphere [*Thompson and Wallace*, 2000].

4. Discussion

[29] We performed CCA on several other seasonal averages of predictor/predictand pairs in order to identify additional direct and lagged relationships: Winter and extended winter (December to May) temperatures with spring and growing season NDVI, summer temperatures with summer NDVI, fall temperatures with fall NDVI, and growing season temperatures with growing season NDVI. The time series of the resulting coupled spatial patterns were less correlated and less robustly associated with the

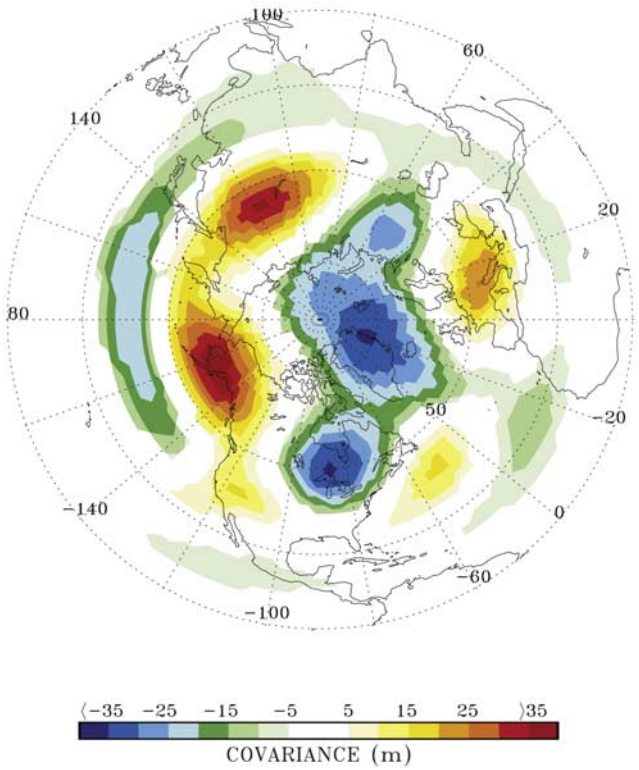

Figure 8. Correlations between spring 250 mbar geopotential height anomalies and the second temporal canonical factor of spring land surface temperature anomalies for 1982 to 1998.

circulation anomalies, suggesting that NH plant growth responds most strongly to contemporaneous variations in temperature during the spring season and that the dominant impact of ENSO and AO is on spring temperatures and vegetation activity.

[30] In addition, we repeated the CCA analysis over the same NH spatial domain and for the identical seasonal pairs but replacing temperature with precipitation [*Xie and Arkin*, 1997] as the predictor. The results (not shown) indicate that the time series of the coupled spatial patterns were not as strongly correlated, and their association to ENSO and AO was not as clear as in the case of temperature. The leading CFs also exhibited sensitivity to EOF truncation. These findings may be explained in part by the fact that over the NH continents water is generally not as strong of a limiting factor for plant growth as temperature [*Los et al.*, 2001]. Besides, ENSO- and AO-like precipitation anomalies are more localized and stronger during the colder seasons (see Appendix B) when their effect on plant growth is predominantly indirect through the timing of snowmelt.

5. Conclusions

[31] In a progressively warming and greening world [*Folland et al.*, 2001; *Keeling et al.*, 1996; *Myneni et al.*, 1997; *Tucker et al.*, 2001] it is important to understand how changes in vegetation activity are correlated with changes in near-surface climate variables such as air temperature [*Zhou et al.*, 2001]. To investigate this issue, we performed a canonical correlation analysis on spring land surface temperature and greenness data to isolate and identify well correlated modes of spatiotemporal variability on regional to hemispheric scales for the period 1982 to 1998. It is found that, during the critical springtime period, spatiotemporal structures in hemispheric-scale vegetation activity are highly correlated with overlying patterns of surface temperatures. In addition, it is shown that surface temperature signatures associated with two predominant modes of global climate variability, namely the El Niño-Southern Oscillation (ENSO) and the Arctic Oscillation (AO), are also the principal drivers for interannual variability in Northern Hemisphere greenness. Additional results indicate that hemispheric-scale upper-air circulation patterns associated with the ENSO and the AO are partly responsible for the correlation between year-to-year changes in spring temperature and greenness in the north.

[32] In general, it is found that during warm ENSO events, warmer and greener conditions prevail in the spring over North America, Far East Asia and to some extent over Europe. Likewise, during the positive phase of the AO, warmer and greener spring conditions prevail in Europe and Asian Russia, and the opposite conditions in the well vegetated eastern half of North America. Interestingly, over the past two decades, warm ENSO events were more frequent and the AO was more often in its positive phase compared to longer historical records [*Trenberth and Hoar*, 1997; *Thompson et al.*, 2000]. In addition, over this period the northern latitude greening reports indicate a more persistent vegetative activity in Eurasia relative to North America [*Schwartz*, 1998; *Zhou et al.*, 2001; *Chmieliewski and Roetzer*, 2002]. The spatial coherence of these pattern to those described above suggest that individual or combined vegetation responses to secular trends in the ENSO and AO teleconnection modes may have contributed to the observed changes in photosynthetic activity. An investigation of this hypothesis is presently being conducted.

Appendix A: Canonical Correlation Analysis

[33] The canonical correlation analysis (CCA) performed in this study is similar to simple EOF analysis, only the field on which the singular value decomposition is performed differs in that it contains a cross-correlation matrix relating the predictand field to the predictor field. A valuable reference for CCA is *Cooley and Lohnes* [1971]. Other descriptions are given by *Barnett and Preisendorfer* [1987] and *Cherry* [1996]. A comparison of CCA with other multivariate analysis techniques is given by *Bretherton et al.* [1992].

[34] To perform CCA, we first compute the empirical orthogonal functions (EOFs) for each data set. The data set is essentially grid box temperature and NDVI anomalies with respect to the 17 year period of record, 1982 to 1998. For the NDVI field, only vegetated pixels, defined as those with monthly NDVI values greater than 0.1 [*Zhou et al.*, 2001], were utilized. For the temperature field, the anomalies for each grid box were normalized by their standard deviation to de-emphasize extreme temperature variability in the far-north. The resulting anomalies were then area-weighted, with the square root of the respective grid box area, to avoid geometrical effects [*North et al.*, 1982].

[35] We then selected the first six EOFs of Northern Hemisphere (10°N to 90°N) spring (March through May)

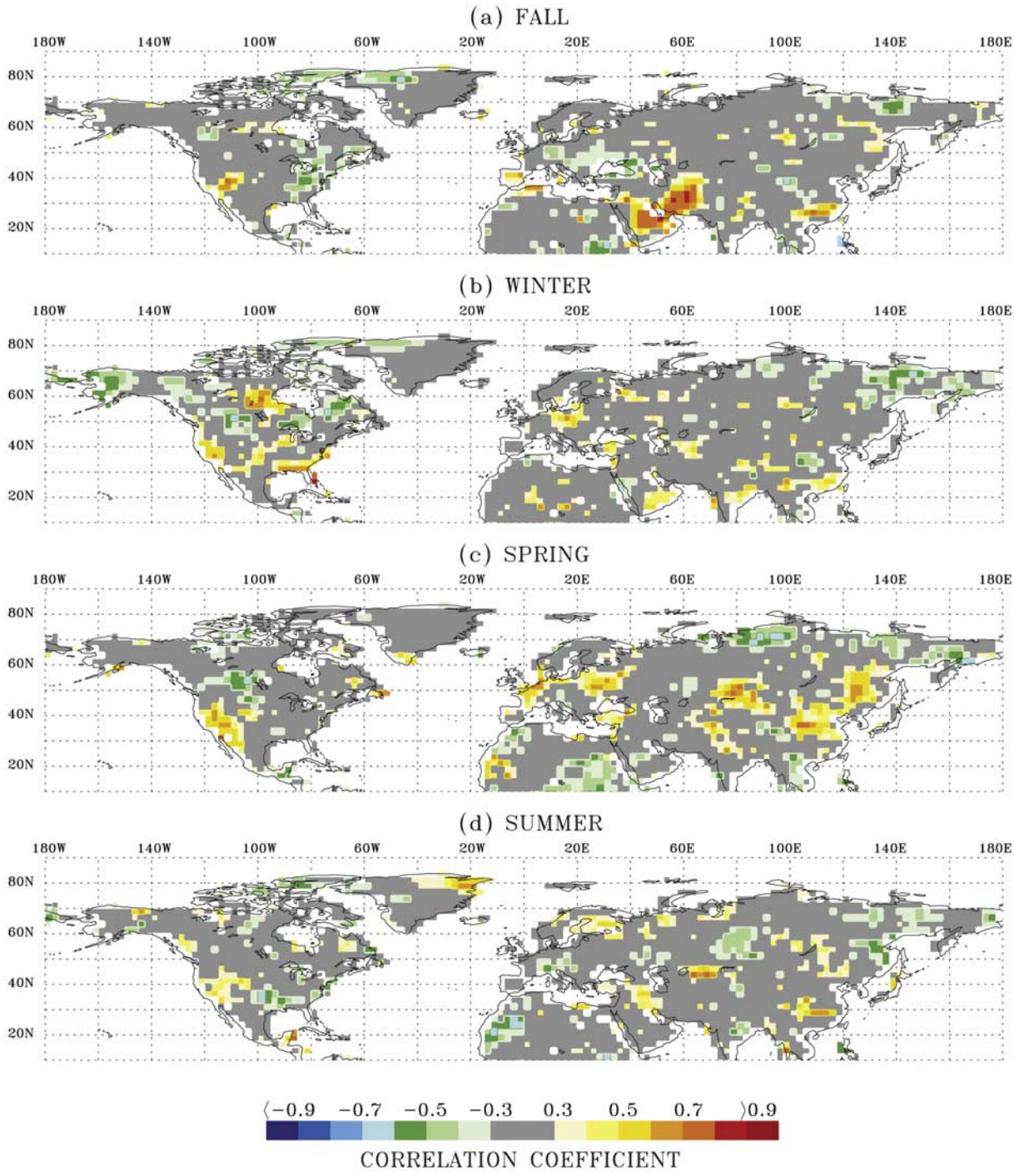

Figure B1. Patterns of simple correlation between September through November average NINO3 index and land precipitation anomalies for the period 1981/1982 to 1997/1998. The four panels depict correlation patterns between 1981 to 1997 September through November average NINO3 and (a) 1981 to 1997 September through November average precipitation anomalies, (b) 1982 to 1998 December through February average precipitation anomalies, (c) 1982 to 1998 March through May average precipitation anomalies, and (d) 1982 to 1998 June through August average precipitation anomalies. Land areas not contoured indicate missing data.

land surface temperature fields and the first six EOFs of NH (10°N to 90°N) NDVI fields. The next step is evaluation of the cross-covariance matrix between these truncated sets of predictor time series (land surface temperature EOFs) and the predictand time series (NDVI EOFs); the same procedure can be performed with the designations reversed with no loss of generality. The autocorrelation matrix for each field is also required. This

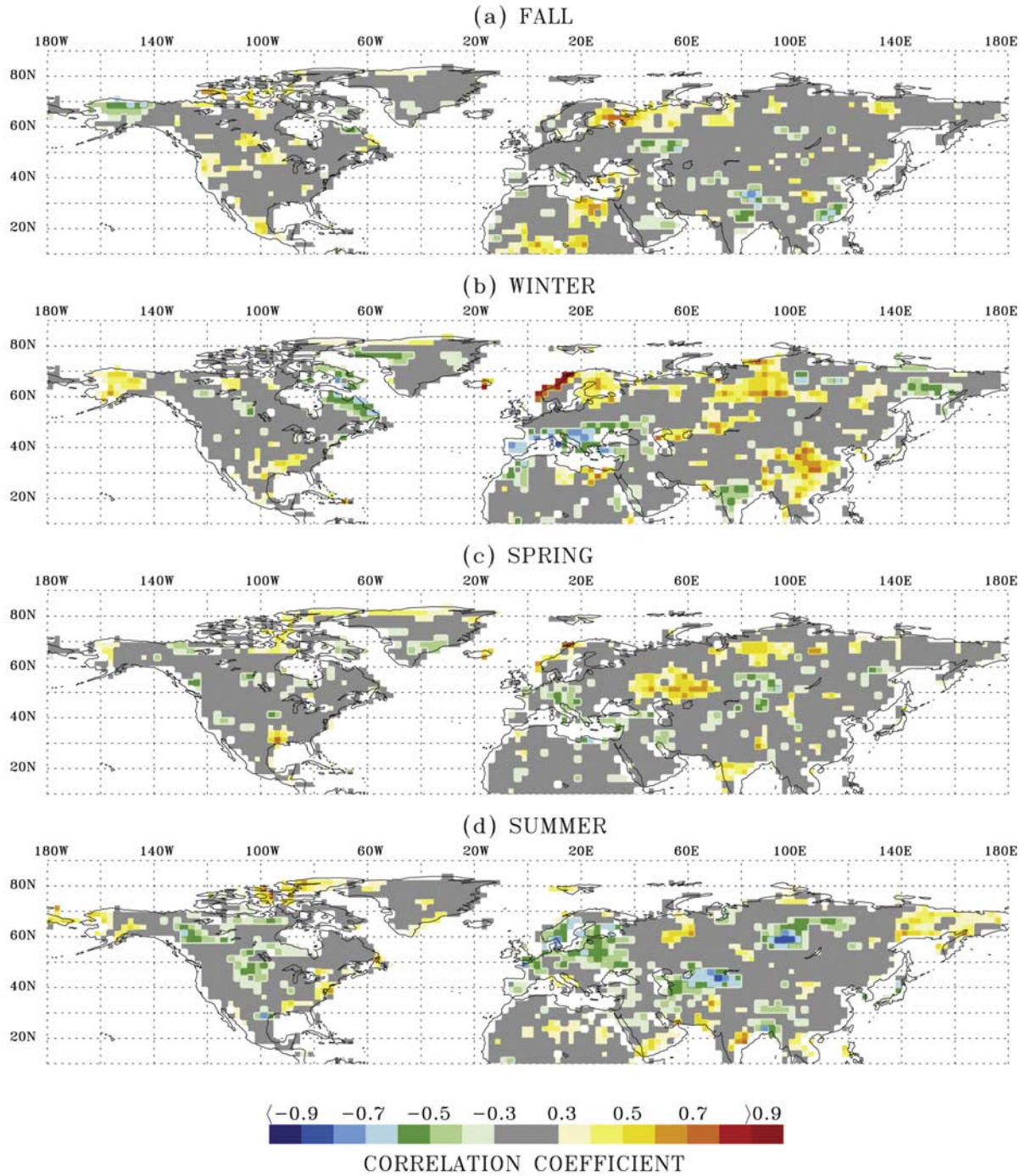

Figure B2. Patterns of simple correlation between three-month averages of the AO index and land surface precipitation anomalies for the period 1981/1982 to 1997/1998. (a) September through November average precipitation anomalies correlated with the JJA AO index for 1981 to 1997, (b) December through February average precipitation anomalies correlated with the DJF AO index for 1982 to 1998, (c) March through May average precipitation anomalies correlated with the JFM AO index for 1982 to 1998, and (d) June through August average precipitation anomalies correlated with the JJA AO index for 1982 to 1998. Land areas not contoured indicate missing data.

matrix is simply a diagonal matrix that normalizes the values in the cross-covariance matrix because the time series are taken from the EOF analysis. Given this truncated set of EOF time series, weighted by the respective eigenvalues, for the land surface temperatures $\overleftrightarrow{T}$ and the NDVIs $\overleftrightarrow{N}$, in which rows represent position in time and columns represent position in EOF-space, a cross-correlation matrix $\langle TN \rangle$ can be calculated as the inner

product $\overleftrightarrow{T}'\overleftrightarrow{N}$ and auto-correlation matrices $\langle TT\rangle$ and $\langle NN\rangle$ as $\overleftrightarrow{T}'\overleftrightarrow{T}$ and $\overleftrightarrow{N}'\overleftrightarrow{N}$, where ($\langle\rangle$) represents the expectation operator. The matrix equation to be solved is $(\langle TT\rangle^{-1}\langle TN\rangle\langle NN\rangle^{-1}\langle TN\rangle' - \lambda)\leftrightarrow A = 0$, where λ represents the diagonal matrix of eigenvalues (equal to the squared correlation of the reconstructed time series) and $\overleftrightarrow{A}$ represents a transformation matrix that is used to reconstruct the time series of the canonical factors (CFs) from the EOF time series. The elements of $\overleftrightarrow{A}$, whose rows represent position in EOF-space and columns represent position in CF-space, give the weighting of each of the original predictand EOFs that comprise the CF time series. Hence, to calculate the CF time series of the predictand, the NDVI pattern $\overleftrightarrow{N}*$, the original weighted time series is multiplied by the transformation matrix, i.e., $\overleftrightarrow{N}* = \overleftrightarrow{N}\overleftrightarrow{A}$. To calculate the corresponding spatial patterns, it is assumed that the reconstructed anomaly field should be equal to the anomaly field represented by the original EOFs, i.e., $\overleftrightarrow{X}*\overleftrightarrow{X}*' = \overleftrightarrow{X}\overleftrightarrow{N}'$ where $\overleftrightarrow{X}*$ and $\overleftrightarrow{X}$ represent the spatial CF and EOF patterns for the NDVI anomalies, respectively. Hence $\overleftrightarrow{X}* = (\overleftrightarrow{X}\overleftrightarrow{N}')(\overleftrightarrow{N}*')^{-1}$.

Appendix B: Precipitation Correlation Maps

[36] In Figures B1 and B2, we present supplementary results on the El Niño-Southern Oscillation (ENSO) and Arctic Oscillation (AO) influences on NH land precipitation. The analysis is similar to that decribed in section 2.2.1, except that precipitation fields are correlated with the respective large-scale circulation indices. In this case, the data were also detrended prior to correlation analysis to reduce the likelihood of spurious correlation (see also *Trenberth and Caron* [2000] for complementary discussion).

[37] **Acknowledgments.** This work was funded by the National Aeronautics and Space Administration Earth Science Enterprise. We would like to thank three unknown reviewers for their helpful comments and suggestions.

References

Arkin, P. A., The relationship between interannual variability in the 200mb tropical wind field and the southern oscillation, *Mon. Weather Rev.*, *110*, 1393–1404, 1982.

Barber, V. A., G. P. Juday, and B. P. Finney, Reduced growth of Alaska white spruce in the twentieth century from temperature-induced drought stress, *Nature*, *405*, 668–672, 2000.

Barford, C. C., S. C. Wofsy, M. L. Goulden, J. W. Munger, E. H. Pyle, S. P. Urbanski, L. Hutyra, S. R. Saleska, D. Fitzjarrald, and K. Moore, Factors controlling long- and short-term sequestration of atmospheric CO_2 in a mid-latitude forest, *Science*, *294*, 1688–1691, 2001.

Barnett, T. P., and R. Preisendorfer, Origins and levels of monthly and seasonal forecast skill for United States surface air temperatures determined by canonical correlation analysis, *Mon. Weather Rev.*, *115*, 1825–1850, 1987.

Bonsal, B. R., A. Shabbar, and K. Higuchi, Impacts of low frequency variability modes on Canadian winter temperature, *Int. J. Climatol*, *21*, 95–108, 2001.

Bradley, N. L., A. C. Leopold, J. Ross, and W. Huffaker, Phenological changes reflect climate change in Wisconsin, *Proc. Natl. Acad. Sci. U.S.A.*, *96*, 9701–9704, 1999.

Braswell, B. H., D. S. Schimel, E. Linder, and B. Moore, The response of global terrestrial ecosystems to interannual temperature variability, *Science*, *278*, 870–872, 1997.

Bretherton, C. S., C. Smith, and J. M. Wallace, An intercomparison of methods for finding coupled patterns in climate data, *J. Clim.*, *5*, 541–560, 1992.

Buermann, W., J. Dong, X. Zeng, R. B. Myneni, and R. E. Dickinson, Evaluation of the utility of satellite-based vegetation leaf area index data for climate simulations, *J. Clim.*, *14*, 3536–3550, 2001.

Cherry, S., Singular value decomposition analysis and canonical correlation analysis, *J. Clim.*, *9*, 2003–2009, 1996.

Chmieliewski, F.-M., and T. Roetzer, Annual and spatial variability of the beginning of growing season in Europe in relation to air temperature changes, *Clim. Res.*, *19*, 257–264, 2002.

Colombo, S. J., Climatic warming and its effect on bud burst and risk of frost damage to white spruce in Canada, *For. Chron.*, *74*, 567–577, 1998.

Cooley, W. W., and P. R. Lohnes, *Multivariate Data Analysis*, 364 pp., John Wiley, New York, 1971.

Dai, A., I. Y. Fung, and A. D. Del Genio, Surface observed global land precipitation variations during 1900–88, *J. Clim.*, *10*, 2943–2962, 1997.

Feddersen, H., A. Navarra, and M. N. Ward, Reduction of model systematic error by statistical corrections for dynamical seasonal predictions, *J. Clim.*, *12*, 1974–1989, 1999.

Folland, C. K., et al., Observed climate variability and change, in *Climate Change 2001: The Scientific Basis*, pp. 101–181, Cambridge Univ. Press, New York, 2001.

Fraedrich, K., An ENSO impact on Europe?, *Tellus, Ser. A*, *46*, 541–552, 1994.

Gill, A. E., *Atmosphere-Ocean Dynamics*, 662 pp., Academic, San Diego, Calif., 1982.

Goulden, M. L., et al., Sensitivity of boreal forest carbon balance to soil thaw, *Science*, *279*, 214–217, 1998.

Halpert, M. S., and C. F. Ropelewski, Surface-temperature patterns associated with the Southern Oscillation, *J. Clim.*, *5*, 577–593, 1992.

Hansen, J., R. Ruedy, J. Glascoe, and M. Sato, GISS analysis of surface temperature change, *J. Geophys. Res.*, *104*, 30,997–31,022, 1999.

Horel, J. D., and J. M. Wallace, Planetary scale atmospheric phenomena associated with the Southern Oscillation, *Mon. Weather Rev.*, *109*, 813–829, 1981.

Hoskins, B. J., and F.-F. Jin, The initial value problem for tropical perturbations to a baroclinic atmosphere, *Q. J. R. Meteorol. Soc.*, *117*, 299–317, 1991.

Hurrell, J. W., Decadal trends in the North Atlantic oscillation regional temperatures and precipitation, *Science*, *269*, 676–679, 1995.

Jarvis, P., and S. Linder, Botany: Constraints to growth of boreal forests, *Nature*, *405*, 904–905, 2000.

Kalnay, E., et al., The NCEP/NCAR 40-year reanalysis project, *Bull. Am. Meteorol. Soc.*, *77*, 437–470, 1996.

Kaufmann, R. K., L. Zhou, Y. Knyazikhin, N. V. Shabanov, R. B. Myneni, and C. J. Tucker, Effect of orbital drift and sensor changes on the time series of AVHRR vegetation index data, *IEEE Trans. Geosci. Remote Sens.*, *38*, 2584–2597, 2000.

Keeling, C. D., J. F. S. Chin, and T. P. Whorf, Increased activity of northern vegetation inferred from atmospheric CO_2 measurements, *Nature*, *382*, 146–149, 1996.

Kiladis, G. N., and H. F. Diaz, Global climatic anomalies associated with extremes in the Southern Oscillation, *J. Clim.*, *2*, 1069–1090, 1989.

Los, S. O., G. J. Collatz, P. J. Sellers, C. M. Malmstroem, N. H. Pollack, R. S. DeFries, L. Bounoua, M. T. Parris, C. J. Tucker, and D. A. Dazlich, A global 9-year biophysical land surface dataset from NOAA AVHRR data, *J. Hydrometeorol.*, *1*, 183–199, 2000.

Los, S. O., G. J. Collatz, L. Bounoua, P. J. Sellers, and C. J. Tucker, Global interannual variations in sea surface temperature and land surface vegetation, air temperature, and precipitation, *J. Clim.*, *14*, 1535–1550, 2001.

Mann, M. E., R. S. Bradley, and M. K. Hughes, Northern Hemisphere temperatures during the past millennium: Inferences, uncertainties, and limitations, *Geophys. Res. Lett.*, *26*, 759–762, 1999.

Menzel, A., and P. Fabian, Growing season extended in Europe, *Nature*, *397*, 659, 1999.

Myneni, R. B., F. G. Hall, P. J. Sellers, and A. L. Marshak, The interpretation of spectral vegetation indexes, *IEEE Trans. Remote Sens.*, *33*, 481–486, 1995.

Myneni, R. B., C. D. Keeling, C. J. Tucker, G. Asrar, and R. R. Nemani, Increased plant growth in the northern high latitudes from 1981 to 1991, *Nature*, *386*, 698–702, 1997.

Myneni, R. B., J. Dong, C. J. Tucker, R. K. Kaufmann, P. E. Kauppi, J. Liski, L. Zhou, V. Alexeyev, and M. K. Hughes, A large carbon sink in the woody biomass of northern forests, *Proc. Natl. Acad. Sci. U.S.A.*, *98*, 14,784–14,789, 2001.

North, G. R., T. L. Bell, R. F. Cahalan, and F. J. Moeng, Sampling errors in the estimation of empirical orthogonal functions, *Mon. Weather Rev.*, *110*, 699–706, 1982.

Parmesan, C., et al., Poleward shifts in geographical ranges of butterfly species associated with regional warming, *Nature*, *399*, 579–583, 1999.

Reynolds, R. W., and T. M. Smith, Improved global sea surface temperature analyses using optimum interpolation, *J. Clim.*, *7*, 929–948, 1994.

Schwartz, M. D., Green-wave phenology, *Nature*, *394*, 839–840, 1998.

Thomas, C. D., and J. J. Lennon, Birds extend their ranges northwards, *Nature*, *399*, 213, 1999.

Thompson, D. W. J., and J. M. Wallace, The Arctic oscillation signature in the wintertime geopotential height and temperature fields, *Geophys. Res. Lett.*, *25*, 1297–1300, 1998.

Thompson, D. W. J., and J. M. Wallace, Annular modes in the extratropical circulation. part I: Month-to-month variability, *J. Clim.*, *13*, 1000–1017, 2000.

Thompson, D. W. J., and J. M. Wallace, Regional climate impacts of the Northern Hemisphere annular mode and associated climate trends, *Science*, *293*, 85–89, 2002.

Thompson, D. W. J., J. M. Wallace, and G. C. Hegerl, Annular modes in the extratropical circulation. part II: Trends, *J. Clim.*, *13*, 1018–1035, 2000.

Trenberth, K. E., and J. M. Caron, The Southern Oscillation revisited: Sea level pressures, surface temperatures, and precipitation, *J. Clim.*, *13*, 4358–4365, 2000.

Trenberth, K. E., and T. J. Hoar, El Niño and climate change, *Geophys. Res. Lett.*, *24*, 3057–3060, 1997.

Trenberth, K. E., and J. W. Hurrell, Decadal atmosphere-ocean variations in the Pacific, *Clim. Dyn.*, *9*, 303–319, 1994.

Trenberth, K. E., and D. A. Paolino, Characteristic patterns of variability of sea level pressure in the Northern Hemisphere, *Mon. Weather Rev.*, *109*, 1169–1189, 1981.

Trenberth, K. E., G. W. Branstator, D. Karoly, A. Kumar, N.-C. Lau, and C. Ropelewski, Progress during TOGA in understanding and modeling global teleconnections associated with tropical sea surface temperatures, *J. Geophys. Res.*, *103*, 14,291–14,324, 1998.

Tucker, C. J., D. A. Slayback, J. E. Pinzon, S. O. Los, R. B. Myneni, and M. G. Taylor, Higher northern latitude normalized difference vegetation index and growing season trends from 1982 to 1999, *Int. J. Biometeorol.*, *45*, 184–190, 2001.

Tucker, C. J., R. Mahoney, N. El-Saleous, S. O. Los, M. Brown, M. Paris, D. Grant, and A. Morahan, The global inventory mapping and monitoring study 1981–1999 AVHRR 8-km data set, *Int. J. Remote Sens.*, in press, 2003.

Vaganov, E. A., M. K. Hughes, A. V. Kirdyanov, F. H. Schweingruber, and P. P. Silkin, Influence of snowfall and melt timing on tree growth in subarctic Eurasia, *Nature*, *400*, 149–151, 1999.

Wallace, J. M., North Atlantic Oscillation/Northern Hemisphere annular mode: Two paradigms: One phenomenon, *Q. J. R. Meteorol. Soc.*, *126*, 791–805, 2000.

Wallace, J. M., and D. S. Gutzler, Teleconnections in the geopotential height field during the Northern Hemisphere winter, *Mon. Weather Rev.*, *109*, 784–812, 1981.

Wang, B., R. Wu, and X. Fu, Pacific-East Asian teleconnection: How does ENSO affect East Asian climate?, *J. Clim.*, *13*, 1517–1536, 2000.

Xie, P., and P. A. Arkin, Global precipitation: A 17-year monthly analysis based on gauge observations, satellite estimates, numerical model outputs, *Bull. Am. Meteorol. Soc.*, *78*, 2539–2558, 1997.

Zhou, L., C. J. Tucker, R. K. Kaufmann, D. Slayback, N. V. Shabanov, and R. B. Myneni, Variations in northern vegetation activity inferred from satellite data of vegetation index during 1981 to 1999, *J. Geophys. Res.*, *106*, 20,069–20,083, 2001.

B. Anderson and R. B. Myneni, Department of Geography, Boston University, 675 Commonwealth Avenue, Boston, MA 02215-1401, USA. (brucea@bu.edu; rmyneni@bu.edu)

W. Buermann, Center for Atmospheric Sciences, University of California, Berkeley, 150 Hilgard, Berkeley, CA 94720, USA. (buermann@atmos.berkeley.edu)

R. E. Dickinson, School of Earth and Atmospheric Sciences, Georgia Institute of Technology, 221 Bobby Dodd Way, Atlanta, GA 30332-0340, USA. (robted@eas.gatech.edu)

W. Lucht, Potsdam Institute for Climate Impact Research, Postfach 601203, 14412 Potsdam, Germany. (wolfgang.lucht@pik-potsdam.de)

C. S. Potter, Ecosystem Science and Technology Branch, NASA Ames Research Center, Mail Stop 242-4, Moffett Field, CA 94035, USA. (cpotter@gaia.arc.nasa.gov)

C. J. Tucker, Biospheric Sciences Branch, NASA Goddard Space Flight Center, Code 923, Greenbelt, MD 20771, USA. (compton@ltpmail.gsfc.nasa.gov)